4-1-1994

Phase Diagram of the Dilute Ising Spin Glass in General Spatial Dimension

Shye Shapira

Lior Klein

Joan Adler

Amnon Aharony

A. Brooks Harris
University of Pennsylvania, harris@sas.upenn.edu

Phase Diagram of the Dilute Ising Spin Glass in General Spatial Dimension

Abstract

We use high-temperature and low-concentration series to treat the dilute spin glass within a model with nearest-neighbor interactions which randomly assume the values $+J$, 0, $-J$ with probabilities $p/2$, $1-p$, $p/2$, respectively. Using the Harris no-free-end diagrams scheme in general spatial dimension, we obtained 15th-order series for χ^{EA} as a function of temperature for arbitrary dilution, 14th-order series for χ^{EA} as a function of dilution for selected temperatures, and 11th-order series for two higher derivatives of χ^{EA} with respect to the ordering field, where χ^{EA} is the Edwards-Anderson spin-glass susceptibility. Analysis of these series yields values of $T_{SG}(p)$, the critical temperature as a function of the dilution p or the analogous critical concentration $p_{SG}(T)$. Thus we determine a critical line, separating the spin-glass phase from the paramagnetic phase in the T-p plane. We find values of the critical exponent γ and universal amplitude ratios along the critical line. Universal amplitude ratios and dominant exponents along the critical line are identical to those of the pure spin glass for a wide range of dilution, indicating the same critical behavior as that of the pure spin glass.

Disciplines
Physics

Phase diagram of the dilute Ising spin glass in general spatial dimension

Shye Shapira
Department of Physics, Technion-IIT, 32000, Haifa, Israel

Lior Klein*
School of Physics and Astronomy, Beverly and Raymond Sackler Faculty of Exact Sciences, Tel Aviv University, 69978, Tel Aviv, Israel

Joan Adler
Department of Physics, Technion-IIT, 32000, Haifa, Israel
and School of Physics and Astronomy, Beverly and Raymond Sackler Faculty of Exact Sciences, Tel Aviv University, 69978,
Tel Aviv, Israel

Amnon Aharony
School of Physics and Astronomy, Beverly and Raymond Sackler Faculty of Exact Sciences, Tel Aviv University, 69978, Tel Aviv, Israel

A. B. Harris
Department of Physics, University of Pennsylvania, Philadelphia, Pennsylvania 19104
(Received 20 July 1992; revised manuscript received 27 July 1993)

We use high-temperature and low-concentration series to treat the dilute spin glass within a model with nearest-neighbor interactions which randomly assume the values $+J$, 0, $-J$ with probabilities $p/2$, $1-p$, $p/2$, respectively. Using the Harris no-free-end diagrams scheme in general spatial dimension, we obtained 15th-order series for χ^{EA} as a function of temperature for arbitrary dilution, 14th-order series for χ^{EA} as a function of dilution for selected temperatures, and 11th-order series for two higher derivatives of χ^{EA} with respect to the ordering field, where χ^{EA} is the Edwards-Anderson spin-glass susceptibility. Analysis of these series yields values of $T_{SG}(p)$, the critical temperature as a function of the dilution p or the analogous critical concentration $p_{SG}(T)$. Thus we determine a critical line, separating the spin-glass phase from the paramagnetic phase in the T-p plane. We find values of the critical exponent γ and universal amplitude ratios along the critical line. Universal amplitude ratios and dominant exponents along the critical line are identical to those of the pure spin glass for a wide range of dilution, indicating the same critical behavior as that of the pure spin glass.

I. INTRODUCTION

The critical behavior of the dilute Ising spin glass (DISG) has attracted the attention of many authors.[1-12] In this paper we further discuss the DISG that is defined by the Hamiltonian

$$\mathcal{H} = -\sum_{\langle ij \rangle} J_{ij} S_i S_j - H \sum_i S_i , \qquad (1.1)$$

where $\langle ij \rangle$ denotes a sum over pairs of nearest-neighbor sites ij, on a hypercubic lattice in d spatial dimensions, and $S_i = \pm 1$. The nearest-neighbor exchange variables $J_{ij} = J_{ji}$ independently assume the quenched values $J, 0, -J$ with the probabilities $p/2, 1-p, p/2$, respectively. In Eq. (1.1) we also include the effect of a uniform nonrandom external field H. Since the J_{ij}'s are quenched variables, the quenched averaged free energy per spin, F, is given by

$$F = -(kT/N)[\ln \text{Tr} e^{-\beta \mathcal{H}}]_{av} , \qquad (1.2)$$

where $\beta = (kT)^{-1}$, $[\ ]_{av}$ denotes an average over all configurations of the J_{ij}'s and N is the total number of spins. Our DISG is of considerable interest as it has a

temperature-dilution-dimension phase diagram which is quite distinct from that of other well-known dilute models in several aspects.

Before discussing the atypical features of the DISG, let us outline some typical temperature-dilution scenarios. Undiluted ferromagnetic spin systems, such as Ising or Heisenberg models, exhibit ordered states in d greater than the lower critical dimension d_{LC} for temperatures less than a critical temperature T_c. Fluctuation-dominated transitions (with non-mean-field exponents) occur in dimensions below the upper critical dimension d_{UC} (which is 4 for Ising and Heisenberg systems). As dilution is progressively introduced, the critical temperature $T_c(p)$ is depressed, reaching zero at the geometrical percolation[13] threshold p_c. In the Ising case, the nature of the critical point changes for $p_c \leq p < 1$ since there is a new random fixed point[14] for finite disorder. Both the Ising and Heisenberg models exhibit percolation critical exponents[2,13] near the zero-temperature critical point at p_c. The Harris criterion[15] differentiates between cases such as the Ising model, where the behavior is determined by a new random fixed point for finite disorder, and cases such as the Heisenberg model where it is not. There are some other families[16] of dilute systems such as the Baxter-Wu

model, certain classical antiferromagnets and quadrupolar structures, where a finite-temperature transition does not occur for a nonzero range of concentration $p_c < p < x_c$. In one of the classical antiferromagnet cases,[17] percolation exponents nevertheless seem to be observed at the $T=0$ transition. In the Baxter-Wu and quadrupolar cases, no study of this has yet been undertaken. In some other models,[18] one observes different thresholds and different exponents.

The nondilute Ising spin glass differs from the nondilute systems discussed in the preceding paragraph because there is already a significant degree of randomness at $p=1$. The value of d_{UC} is raised to 6 and d_{LC} is now believed[19,20] to be 3. Debate concerning the latter question was long and contentious. Therefore there is a question of principle to determine what effect further randomness of dilution will have. Our group has recently carried out series-expansion studies of both the $p=1$ limit[12] and the $T=0$ limit[20] of the DISG. In the former we made a careful analysis of all dimensions between 3 and 6. Our $d=5$ results gave a substantially more accurate description of the critical behavior than had previously been attained below d_{UC}. These results were the first series to confirm the prediction of Ref. 10 that the zero-temperature transitions occurred at a threshold p_{SG} higher than the geometrical threshold p_c. We also attempted to determine the nature of the $T=0$ DISG transition and gave a summary of the history of this problem in detail in Ref. 12. Briefly, one follows the "replica trick" approach of Stephen and Grest[2] to the $T=0$ limit for the dilute Ising model. They used the generalized susceptibilities $\chi^{(q)} = \sum_i [\langle S_i S_j \rangle^q]_{av}$, where [ ] and $\langle \rangle$ denote configurational and thermal averages, respectively. They pointed out that for the $T=0$ dilute Ising model, all the $\chi^{(q)}$'s diverge at the same concentration p_c. Since these $\chi^{(q)}$'s represent 2^n states, the resulting percolation behavior is obtained for $n \to 0$ as the $q \to 1$ limit of the q-state Potts model. For the $T=0$ DISG, Aharony[4] and Giri and Stephen[3] noted that for odd q's $\chi^{(q)}$ vanishes, and they assumed that for even q's all $\chi^{(q)}$ diverge together. Since this corresponds to $2^n - 1$ states, they concluded that the model is equivalent to the $q \to \frac{1}{2}$ limit of the q-state Potts model. It was soon realized, however, that this approach disregarded some frustration effects[6] and therefore yielded incorrect conclusions. Harris[10] showed that in the limit of high dimensions, the $\chi^{(2q)}$'s tend to diverge at $T=0$ at different concentrations $p_c < p_2 < p_4 < \cdots$, $\chi^{(2)}$ tending to diverge at the lowest concentration. However, as soon as $\chi^{(2)}$ diverges at p_2, the higher $\chi^{(2q)}$'s will also diverge, although with weaker singularities. The dominant singularity at the $T=0$ transition of the DISG is thus that of $\chi^{(2)} \propto \chi^{EA}$. Since this is the same singularity as for the nondilute spin glass, Harris predicted nondilute spin-glass behavior for the DISG at all p, including the zero-temperature transition at $p = p_{SG}(T=0)$, which is larger than p_c. Nevertheless, it should be noted that the apparent thresholds of the $\chi^{(q)}$'s are very close and there may be crossover effects from the nearby fixed point of the $\frac{1}{2}$-state Potts model. Some numerical evidence was given to support the exten-

sion of the Harris claim to low dimensions from the $T=0$ studies of Ref. 12. The present calculation has been undertaken in order to further explore Harris' claim for general dilution and temperature and to determine whether there are any intermediate new fixed points, such as occur in the dilute Ising ferromagnet case for finite temperature and dilution.

In order to calculate quenched averages such as that in Eq. (1.2), we introduce the replica Hamiltonian[1]

$$\mathcal{H}^{(n)} = - \sum_{\langle ij \rangle} \sum_{\alpha=1}^{n} J_{ij} S_i^\alpha S_j^\alpha - h \sum_i \sum_{1 \le \alpha < \beta \le n} S_i^\alpha S_i^\beta , \quad (1.3)$$

where h is the field conjugate to the Edwards-Anderson spin-glass (SG) order parameter $Q = [\langle S_i \rangle^2]_{av}$ and there are n replicas. Then we define

$$F_{rep} = \lim_{n \to 0} \left[-\frac{2kT}{n(n-1)N} \ln \text{Tr}[e^{-\beta \mathcal{H}^{(n)}}]_{av} \right] , \quad (1.4)$$

which is related to F of Eq. (1.2) via the relation $F_{rep} = -2F$. We obtained expansions for Γ_k, for $k=2,3,4$, where we define Γ_k as the kth derivative of F_{rep} with respect to the SG ordering field:

$$\Gamma_k = - \left[\frac{\partial^k \beta F_{rep}}{\partial \tilde{h}^k} \right]\Bigg|_{h=0} , \quad k=2,3,4 , \quad (1.5)$$

where $\tilde{h} = \beta h$. In a previous paper,[20] we showed that, in the critical regime,

$$\frac{\partial^{2k} F}{\partial H^{2k}} \sim \frac{-(2k-1)!}{(k-1)!} \left[\frac{1}{k_B T} \right]^{2k-1} \Gamma_k . \quad (1.6)$$

The second derivative Γ_2 is the Edwards-Anderson (EA) susceptibility.[1] In the disordered phase $[p < p_{SG}(T)$ or $T > T_{SG}(p)]$,

$$\Gamma_2 \equiv \chi^{EA} = N^{-1} \sum_{ij} [\langle S_i S_j \rangle^2]_{av} . \quad (1.7)$$

We have studied the critical behavior by computing both universal amplitude ratios[21,22] and critical exponents along the critical line via a general dimension low-concentration and high-temperature series-expansion approach. We have generated 15th-order series in temperature for χ^{EA} for general dimensions and arbitrary concentrations and shorter series for higher derivatives of the free energy. Series to 14th order in p at arbitrary temperature have also been obtained for χ^{EA}. These have enabled us to determine the complete dilution-temperature phase diagram for general dimension. These results suggest that there is no intermediate fixed point and further support the expectation of a pure spin-glass behavior along the entire critical line.

The multiple series for general temperature, dilution, and dimension contain an enormous amount of information. The generation of these series is discussed in detail in Sec. II and in the Appendix. Our algorithm generates the coefficients of the series, in the high-temperature variable $w = \tanh^2(J/kT)$, as explicit polynomials in p and d. Thus a single calculation yields results which then enable

analyses for all p and d. In some sense this may be considered as a "parallel" algorithm. (We use the term parallel in analogy with simulation terminology, where parallelization enables one to calculate many different cases simultaneously with large savings of CPU time.) The entire 15th-order series for χ^{EA} for general dimension and dilution, required only some 100 hours of CPU time on a Cyber 180/990E. When one considers that for a pure spin glass in three dimensions the computation time for simulations on relatively small samples is so enormous that special purpose machines must be built and that dilution substantially increases the number of samples that must be taken, our approach represents an enormous saving of computer time. Unfortunately, the higher derivatives required rather more time even within the "parallel" approach, and therefore we stopped at 11th order, since we mainly required the higher derivatives for amplitude ratios which converge quite well even for the shorter series. The 14th-order series in p for χ^{EA} for a number of temperatures near zero ($w = 1$) took some 50 h on the Cyber 180/990E. These series are also good for all dimensions, but had to be calculated in a scalar mode for different w values. Sufficient coefficients to rebuild all the series are given in Tables I–IV; see APS repository, Ref. 23.

The enormous amount of information contained in the series was first processed via D log Padé-approximant analysis, fitting to the critical behavior

$$\chi^{EA}(w) \sim A(w_c - w)^{-\gamma} \tag{1.8}$$

in order to obtain values of the critical exponent γ and the critical values w_c for given dimensions and a fine grid of concentration values. This grid included some 80 different (p, d) locations. The analysis was undertaken with a specially written, highly automated, and efficient program that was specially prepared for this project. The details of the critical parameters and the resulting phase diagrams in the concentration-temperature plane are given in Sec. III. Similar analyses were made for the series in p, which should diverge with the same γ at the temperature-dependent concentration threshold p_{SG}.

In many cases we found that the dilute models converged better than the pure system, and to research this further at certain especially interesting locations we have also extrapolated these series according to the more detailed critical behaviors

$$\chi^{EA} \sim (p_{GS} - p)^{-\gamma}[1 + a_p(p_{SG} - p)^{\Delta_1}] \tag{1.9}$$

and

$$\chi^{EA} \sim (w_c - w)^{-\gamma}[1 + a_w(w_c - w)^{\Delta_1}] , \tag{1.10}$$

where Δ_1 is an exponent that allows for the effect of confluent corrections to scaling. Details of the special regions and comparisons between dilution and temperature-series results are presented in Sec. IV.

The higher susceptibilities[20] Γ_3 and Γ_4 are expected to diverge with exponents of $\gamma + \Delta$ and $\gamma + 2\Delta$, respectively, where $\Delta = \gamma + \beta$ is known as the gap exponent and β is the order-parameter exponent for $w > w_c$, $[\langle S_i \rangle^2]_{av} \sim (w - w_c)^\beta$. Γ_3 and Γ_4 were studied both to measure the

gap exponents and in order to study the universal amplitude ratio[21,22] for the dilute model. These ratios

$$R \equiv \frac{\Gamma_2 \Gamma_4}{(\Gamma_3)^2} \tag{1.11}$$

were calculated in all dimensions along the critical line. These results are presented in Sec. V. We conclude in Sec. VI with a discussion of the overall implications of our results.

II. GENERATION OF THE SERIES

We have generated the series for Γ_k ($k = 2, 3, 4$) via the Harris[24] scheme that uses only no-free-end (NFE) diagrams. Details on the implementation of this scheme for the pure and zero-temperature dilute spin glasses have already been published.[12,20] We therefore list here and in the Appendixes only our final results. We refer the reader to the discussion in Sec. III of Ref. 20. The basic idea is to write the partition function in the form

$$Z = \text{Tr} \prod_i \rho_i [g(S_i, h)]^z \prod_{\langle ij \rangle} \frac{f_{ij}}{g(S_i, h)g(S_j, h)} , \tag{2.1}$$

where $z = 2d = \sigma + 1$,

$$\rho_i = \exp\left[(h/k_B t) \sum_{\alpha < \beta} S_i^\alpha \cdot S_i^\beta\right] ,$$

$$f_{ij} = \cosh\left[(J/k_B T) \sum_\alpha S_i^\alpha \cdot S_j^\alpha\right] , \tag{2.2}$$

and $g(S_i, h)$ must obey[24]

$$g(S_i, h) = \frac{\text{Tr}_j \{\rho_j [g(S_j, h)]^\sigma f_{ij}\}}{\text{Tr}_j \{\rho_j [g(S_j, h)]^z\}} . \tag{2.3}$$

The essential expansion of $g(S_i, h)$ for the present case is presented in Appendix A. To implement the NFE scheme, we write the Γ_k's according to

$$\Gamma_k = \Gamma_k^{CT} + \sum_\Gamma W_d(\Gamma) \delta\Gamma_k(\Gamma)_c . \tag{2.4}$$

Here Γ_k^{CT} is the calculated susceptibility on a Cayley tree having the same coordination number ($2d$) as the d-dimensional hypercubic lattice, $W_d(\Gamma)$ is the weight of the NFE diagram Γ, and $\delta\Gamma_k(\Gamma)_c$ is the cumulant contribution of this diagram to Γ_k. Explicit expressions for $\delta\Gamma_k(\Gamma)$ are given in Appendix B. The expressions in terms of NFE diagrams are far more complicated than those using a full set of diagrams, especially for Γ_4. Nevertheless, because the fraction of diagrams which have no free ends is very small, there is a very important saving in computer time when NFE diagrams are used.

The series of χ^{EA} at general p expanded in w are listed in Table I (see APS repository)[23] and those for Γ_3 and Γ_4 in Tables II and III, respectively (see APS repository).[23] We define the series coefficients a_k by

$$\Gamma_k = a_k(0,0,0) + \sum_{l=1}^{15} \sum_{m=1}^{15} \sum_{n=1}^{15} a_k(l,m,n)w^l p^m d^n , \tag{2.5}$$

but only nonzero elements are listed in the tables. These series are for arbitrary dimension and concentration.

We cannot obtain a 15th-order series in p for general w. The reason is that the calculation of the coefficients $a_k(l,m,n)$ of Eq. (2.5) involves the division of two polynomials in w. When we generate a double series, we expand this division up to the 15th order. However, if we are interested in a series in p at a given temperature, we must calculate this division exactly. We chose to do this at a few temperatures only, in general dimension, to obtain

$$\Gamma_2 = 1 + \sum_{m=1}^{15} \sum_{n=1}^{m} b_w(m,n) p^m d^n \ . \tag{2.6}$$

The nonzero series elements $b_w(m,n)$ for χ^{EA}, expanded in p at fixed w, are listed in Table IV (see APS repository).[23] To the best of our knowledge, the higher susceptibility and p series are new, and the w series for χ^{EA} [Eq. (2.5)] represent an extension by 5 terms of those of Palmer and Bantilan.[9]

III. PADÉ ANALYSIS
OF THE PHASE DIAGRAM

In the initial stage of our analysis, we studied the 15th-order series for χ^{EA} with the D log Padé analysis. In this method[25] one calculates the Padé approximants to the series of the logarithmic derivative of the susceptibility. To a first approximation, we expect χ^{EA} to have the singular behavior of Eq. (1.8) near the critical point. Therefore the logarithmic derivative of χ^{EA} is expected to have a simple pole at w_c with a residue $-\gamma$:

$$\frac{d \ln \chi^{EA}}{dw} \sim \frac{-\gamma}{(w - w_c)} \ . \tag{3.1}$$

The 14th-order logarithmic derivative series derived from the 15th-order χ^{EA} series yields 105 approximants denoted by P_C^D, $1 \leq D + C \leq 14$ and $0 \leq D$, $1 \leq C$. (The approximant P_C^D is a ratio of two polynomials: one of order D divided by another of order C.) These approximants give 105 different values for w_c and γ, and all 105 can be generated on each of the 80 (d,p) grid points. As a first step, making no assumptions concerning the choice
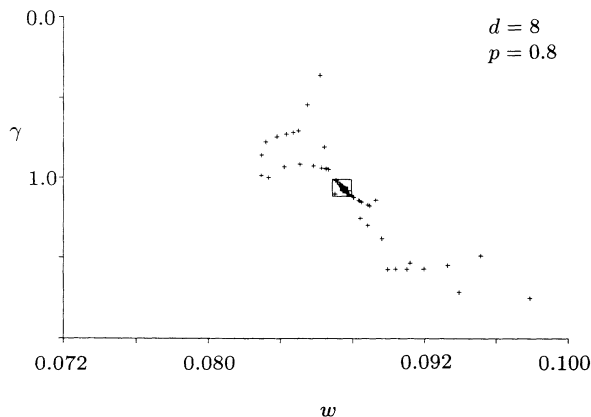

FIG. 1. Graph of the critical temperature $w = \tanh^2(J/kT)$ and critical exponent values obtained via Padé approximants to the logarithmic derivative of the susceptibility series for a bond concentration of $p = 0.8$, at dimension $d = 8$. A box encloses the region of optimal convergence.

of approximants, the values of the approximants were presented on a pole-residue plot for each of the 80 (d,p) grid points. The center of the region with the highest density of approximant values was chosen as the result. An example of such a pole-residue plot for the case of eight dimensions is shown in Fig. 1 for $p = 0.8$. Here the central boxed region (chosen by visual inspection) gives estimates of $\gamma = 1.05 \pm 0.05$ and $w_c = 0.0875 + 0.0005$. This procedure was found to be useful for obtaining an approximate picture of the phase diagrams, but for lower dimensions where the convergence of the approximants is poorer, the boundaries of the region of high density of approximants were blurred and other schemes for interpreting the results had to be considered.

In order to tackle the large amount of data encountered in this project, viz., 105 different values per value of bond concentration per dimension, and to maintain flexibility while automating part of the decision process, a new FORTRAN routine for Padé analysis was written. This routine generates the table of all 105 approximants for given dimension and concentration and places it in a file with a standardized labeling scheme, the label being generated by use of character graphics within the program. All these files are accessible from a single output graphical program written in FORTRAN using DISSPLA graphics. The graphical aspect of the results was especially useful for rapid collating of the approximant data in any desired form. This enabled quick experimentation with different selection schemes for the approximants. This program has become the basis for a new set of series-analysis algorithms, which will be described in detail in Ref. 26.

We found that the best converged alternative to the use of all approximants for estimating values of the exponent γ and transition temperature T_c (or equivalently w_c) is to use the values of 11 high and central approximants denoted by P_7^7, P_6^7, P_7^7 P_8^6, P_7^6, P_6^6, P_5^6, P_8^5, P_7^5, P_6^5, and P_5^5. Graphics of critical temperature and exponent estimates were obtained from the approximant files as a function of concentration of bonds. For high dimensions, $d > d_{UC} = 6$, all 11 values of these approximants are in excellent mutual agreement for both the critical temperature values and the critical exponent values. The values of w_c from these 11 approximants for all bond concentrations at $d = 8, 5, 4$ are presented in Figs. 2(a), 2(b), and 2(c), respectively. In the two higher dimensions $d = 8$ and 5, the values of the 11 approximants are in good mutual agreement, as can be observed in Figs. 2(a) and 2(b). In these dimensions these values are also in good agreement with the values obtained from the average of all the 105 approximants via the pole-residue plots. The average values are represented by the solid lines in the figures. As the dimension is decreased, there is increased dispersion in the approximant values, as Fig. 2(c) demonstrates for $d = 4$. The values of the zero-temperature threshold concentration $p_{SG}(T = 0)$ and the pure system value $w_c(p = 1)$ are compatible with the results obtained for susceptibilities of the zero-temperature dilute[12] and the pure[20] Ising spin glasses, respectively.

The same analysis was also performed on the χ^{EA} series to 14th order in bond concentration for a number of fixed

temperatures $w = 0.87, 0.92, 0.99$. We thereby obtained a second independent set of values of points on the critical line in the neighborhood of zero temperature ($w = 1$). Unfortunately, for dimensions $d = 3, 4, 5$, these values do not coincide with the values obtained from the series in temperature, as can be seen in Fig. 2. A further analysis, allowing corrections to scaling, was carried out on the series in p in order to determine whether this discrepancy is due to the limited length of the series. This analysis is described in Sec. IV.

The values of the high and central approximants for the critical exponent γ also become somewhat dispersed as the dimension decreases. These values for γ along the

critical line are shown in Figs. 3(a), 3(b), and 3(c) for $d = 8$, 5, and 4, respectively. As can be seen in Fig. 3, for $d > 4$ the critical exponent γ has a fairly constant value for bond concentrations greater than $\sim 3p_{SG}(0)$. Although the average is still constant, individual estimates are somewhat dispersed in $d = 4$. At lower bond concentrations, the γ values decrease smoothly and monotonically as p decreases. At the zero-temperature critical bond concentration p_{SG}, the exponent has a value agreeing with the exponents found at the zero-temperature threshold (p_c) values quoted in Ref. 12. In the case of $d = 3$, the graph of γ as a function of concentration shows considerable dispersion in approximant values for
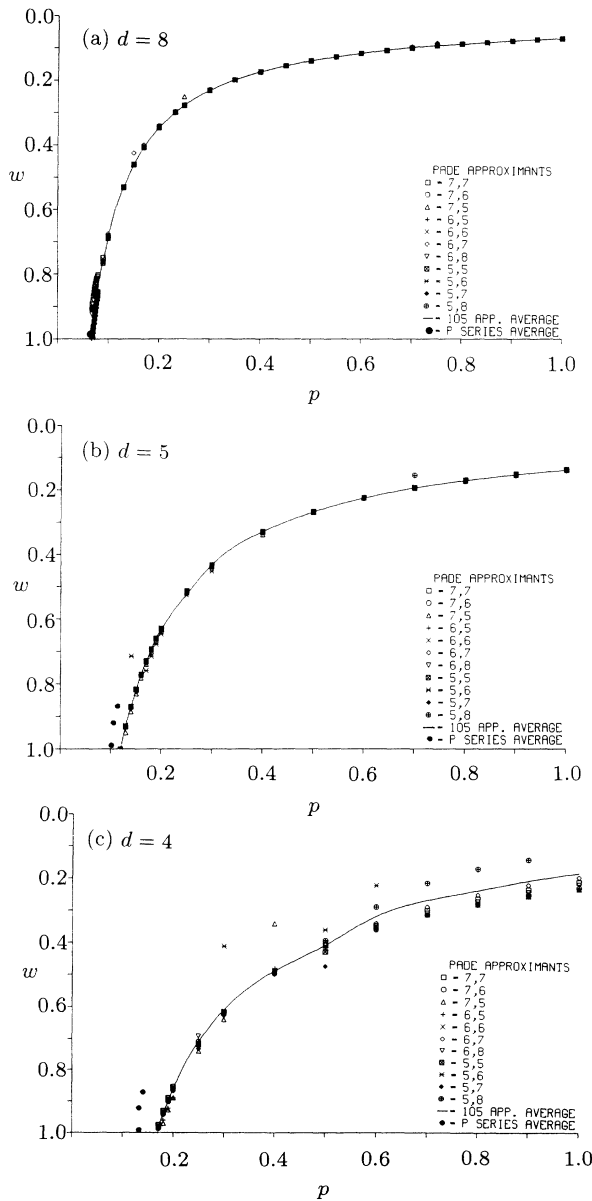

FIG. 2. Phase diagrams for (a) $d = 8$, (b) $d = 5$, and (c) $d = 4$ as obtained from values of 11 high and central approximants. The solid line in each figure represents the average of the estimates obtained from pole-residue plots of all 105 approximants. The solid circles are average results derived from series in the bond concentration p at fixed w.
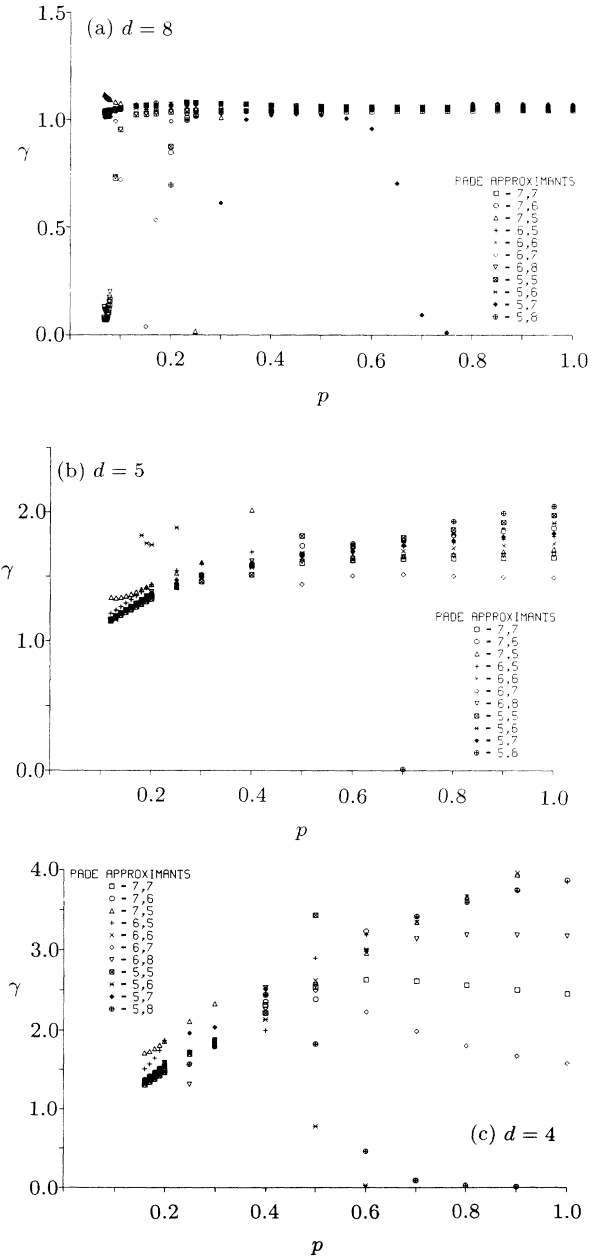
FIG. 3. Padé-approximant estimates of the critical exponent γ as a function of bond concentration for (a) $d = 8$, (b) $d = 5$, and (c) $d = 4$. Values of 11 high and central approximants are shown.

concentrations above $p = 0.5$, with convergence to $\gamma \approx 2.7$ near $p = 0.5$. This graph is not shown and this situation is discussed in detail below.

IV. ADDITIONAL ANALYSES IN SPECIAL REGIONS OF THE PHASE DIAGRAMS

The results of the D log Padé analysis of the high-temperature series in the higher dimensions ($d \geq 5$) are in excellent overall agreement with exact results and with the series for both the pure and zero-temperature systems. There are two notable deviations from internal consistency and agreement of the approximant values. One occurs near the pure limit in three dimensions, where the values of the critical exponent γ and the critical temperature w_c exhibit a large dispersion. This is disturbing, but undoubtedly reflects problems seen also in analyses of the pure system. Just as in the pure system, some slight discrepancies of a similar nature were also observed in $d = 4$.

The second deviation from internal consistency is near the zero-temperature limit in three to five dimensions, where the critical values obtained from series in p and series in w do not mutually agree. This deviation was unexpected and is especially surprising since the simple D log Padé analysis described above does agree with the estimated from the zero-temperature DISG series.

In order to determine whether these two problems reflect any real crossover effects or are merely artifacts of the D log Padé analysis, we have studied the series in these two limits with allowance for corrections to scaling such as appear in Eq. (1.9). Two methods $M1$ and $M2$, which are discussed in depth in Refs. 26–29, have been used. In both these methods, transformations are made to eliminate the effect of corrections to scaling, and then graphs of Padé approximants to the dominant (correction) exponent as a function of trial correction (dominant) exponent are drawn at a trial threshold or temperature value in $M2$ ($M1$). The chosen set of (γ, Δ_1) values is within the region where different approximants give the same results in both methods, and the chosen critical point is that for which optimal convergence is seen. These methods were applied at many different points in the phase diagram, in all dimensions. Excellent agreement with averages of the different approximants was obtained, except for two cases. These two cases were exactly those itemized above. This shows that apart from these cases, where internal inconsistency already gave a signal of trouble, the D log Padé method can give an adequate analysis for many aspects of this model. In particular, this method is substantiated by $M1$ and $M2$ for $d \geq 5$.

In $d = 4$, the more detailed $M1$ and $M2$ analyses gave exponent estimates near $\gamma = 2.0$ for large p values, in agreement with the pure values of Ref. 20 and the average of the dispersed results of the D log Padé analysis. Somewhat surprisingly, convergence is actually better for the more dilute systems. This may be due to the fact that dilution decreases the number of loops and thus may decrease the effects of frustration.

The difference between results in the two directions near $T = 0$ can be seen in Fig. 2; the results from the temperature direction agree with those of Ref. 12 where corrections to scaling were taken into account and disagree with those from the simple Padé analysis in the p direction. In order to explore this discrepancy, the correction to scaling analysis was undertaken for the new series in both directions. Let us consider the four-dimensional case in detail. The simple Padé analysis discussed in Sec. III gives (w_c, p_{SG}) estimates of (0.98,0.17), (0.94,0.18), (0.90,0.19), and (0.86,0.20), for the w series at fixed p leading to a zero-temperature threshold of a little below 0.17 in agreement with the direct value of 0.1645 from Ref. 12. For the p series, the simple method gives (0.99,0.126), (0.92,0.133), and (0.87,0.14), implying a threshold nearer to 0.125. This is substantially below the percolation value ($p_c \approx 0.16$) which is a lower bound on the dilute spin-glass threshold. When the $M1$ and $M2$ analyses were carried out, we found that the effect of corrections on the w series at fixed p was slight and altered the optimal threshold only along the vertical line of the phase-diagram boundary. The threshold remained near 0.17 in all cases. However, for the p series at fixed w, the corrections appear to have a very large effect. For example, let us consider the series at $w = 0.99$. The simple analysis here gives $p_{SG} = 0.126$, with γ being far too low at 0.45. The correction to scaling analysis gives better convergence for $p_{SG} = 0.165$, with $\gamma = 1.2$. Slightly higher thresholds correspond to higher γ values, similar to the results given in Ref. 12 for zero temperature.

V. RESULTS FROM THE HIGHER SUSCEPTIBILITIES

A. Gap exponent

The 11th-order w series for the higher susceptibilities Γ_3 and Γ_4 should diverge with the dominant critical exponents $\gamma + \Delta$ and $\gamma + 2\Delta$, respectively. We carried out estimations of these exponents with the same techniques as used for the χ^{EA} series. From the methods that did not allow for the effects of corrections to scaling, we obtained $\Delta = 2.0$ and thus $\beta = 1$ at $d = 8$. For $d < d_{UC} = 6$, the values of the simple D log Padé analysis were greatly dispersed. For example, in five dimensions the values of $\gamma + \Delta = 2\gamma + \beta$ ranged between 6.2 for the pure spin glass and 3.0 for the zero-temperature critical bond concentration $p_{SG}(w_c = 1)$. Such a continuous variation of exponent as a function of p indicates either an inadequacy in the D log Padé analysis or an insufficiently long series.

Allowance for corrections to scaling improved the situation somewhat; in particular, the $M1$ results were surprisingly good for such short series. For example, at $p = 0.8$ in $d = 5$, we measured $\gamma = 1.72 \pm 0.04$ from $M1$ on χ^{EA} at $w_c = 0.171$ for 15 terms [consistent with the unbiased exponent and temperature results as given above in Figs. 2(b) and 3(b), respectively, from the D log Padé analysis]. For Γ_3 we found $\gamma + \Delta = 4.6 \pm 0.1$ at the same temperature and threshold, implying $\Delta = 2.88 \pm 0.14$ and $\beta = 1.1 \pm 0.14$, using the γ from the longer series. The values for γ from shorter series are higher, leading to a

lower β estimate if used. The results at $p = 0.8$ are typical of those above $p = 0.5$. For $p = 0.4$, where $w_c = 0.33$ gave optimal convergence, we measured $\gamma + \Delta = 4.1$, suggesting that like the γ estimates there is a slow decrease in Δ for concentrations below $p = 0.5$. Overall, the gap exponent measurements are not extremely accurate, but they are consistent with a constant gap exponent, with the same value as that of the pure model values quoted in Ref. 20.

B. Amplitude ratios

Series for the universal amplitude ratios $R \equiv \Gamma_2\Gamma_4/(\Gamma_3)^2$ were obtained by multiplication and division of the 11th-order series in w for Γ_3, Γ_4, and the 11th-order portion of the 15th-order χ^{EA} series. Padé approximants were found for the amplitude-ratio series, and their values were calculated for the corresponding critical temperatures obtained from the Γ_2 analysis. Results for 11 high central approximants are in excellent mutual agreement for $d = 8$ and become dispersed with decreasing dimensions. The values of the 11 high and central approximants are distributed around a constant value, approximately 3 for $d \geq 3$ along the critical line. Our results for $d = 8$, 5, and 4 are given in Fig. 4. In $d = 8$ all the approximant values are in excellent mutual agreement along most of critical line. However, near the $T = 0$ critical point, the values of most of the approximants rise abruptly. This behavior is also noted in four and five dimensions. This behavior persists for $d \gg 8$ as well as for the DISG series on the Cayley-tree lattice. We could find no physical argument for this sudden rise; it is certainly not connected with frustration since the latter is absent from the Cayley tree. It appears to be an effect related to the shortness of the series which causes increased uncertainty, especially as T_{SG} decreases. One possibility is that the rise could be related to some small bias introduced by the finite-series analysis in the $w_c(p)$ values. This may cause a bias in the amplitude-ratio values, proportional to $|dw_c/dp_c|$. This bias would hardly be noted in the high bond concentration regime where $|dw_c/dp_c|$ is very small (Fig. 2), but would be amplified in the vicinity of the zero-temperature critical point where the absolute value of the derivative is the largest. Additional evidence for this correlation between the deviation of the approximant values and the absolute value of the critical temperature to bond concentration derivative can be found when one notes that both this deviation and the increase in the absolute value of the derivative (Fig. 2) grow larger as dimension is increased.

These results must be compared with those for other models, the only available potentially relevant ones being for the pure spin glass and for percolation. (From the discussion in the introduction and in Ref. 12, we do know that there is no physical reason to suspect percolationlike amplitude ratios, but the crossovers near the $T = 0$ critical point give us reason to make comparisons and double-check.) The values of R for the pure spin glass are given in Fig. 4 or Ref. 20 (explicitly 2.77 ± 0.08 at $d = 5$ and 2.8 ± 1.5 at $d = 4$), and those for percolation can be derived from the S ratios in Table VI of Ref. 30.

(We quote the results 2.573, 2.221, and 1.917 for $d = 5$, 4, and 3, respectively, from this table.) From Fig. 4 it is clear that for all concentrations there is a difference between the plotted points for the DISG and the percolation value. The difference persists for all concentrations. There is no crossover towards percolation values for low concentrations as seems to occur for exponents [Fig. 3(b)]. This strongly supports the argument that the critical behavior along the critical line is governed by the pure spin-glass parameters and is different from that of percolation. We must note, however, that an examination of the results[20] for the universal amplitude ratios of the pure Ising spin glass, obtained from a 15th-order
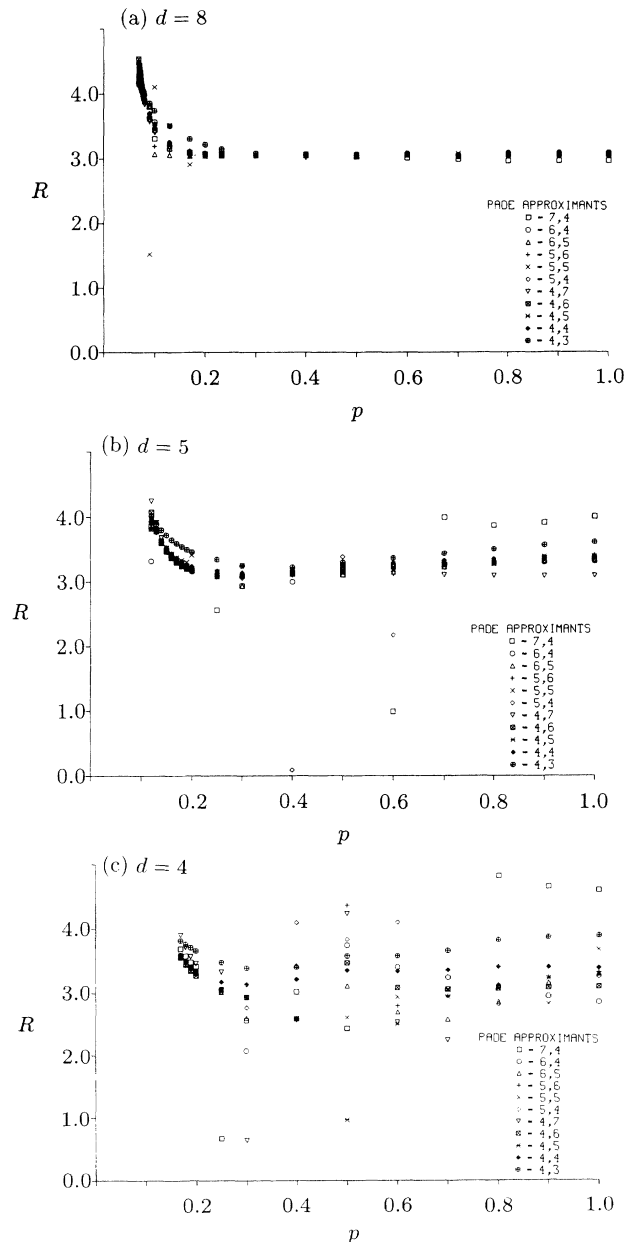

FIG. 4. Values of 11 central and high Padé approximants to the amplitude ratio R for (a) $d = 8$, (b) $d = 5$, and (c) $d = 4$ as a function of bond concentration p.

series in w, reveals that the group of results for high order and central approximants exhibit a bifurcation into two groups of results which makes it hard to determine the value of the result (the numbers quoted above are averages). This behavior could persist in the dilute model and complicate our conclusions.

VI. SUMMARY AND CONCLUSIONS

(1) We studied the critical properties of the dilute Ising spin glass and obtained phase diagrams in the temperature-dilution plane for various spatial dimensions. These results for the transition temperature $T_{SG}(p)$ or the critical concentration $p_{SG}(T)$ may allow for comparison to measurements on nonmetallic spin glasses such as those mentioned in Ref. 31.

(2) As expected, the critical properties and universal amplitude ratios are independent of p. The values of the critical exponents remain constant from $p = 1$ down to $p \approx 3p_{SG}(0)$. The universal amplitude ratio R of Eq. (1.11) was found to be independent of p over almost the entire concentration range down to $p_{SG}(0)$.

(3) Our results are not inconsistent with our previous calculations[12] and with the critical behavior of the dilute Ising spin glass being in the same universality class as the undiluted spin glass, as one would expect from the Harris result.[10]

(4) The critical behavior of the zero-temperature critical point is not that of classical percolation. This is shown both from the critical exponents and from the value of R. Our results are consistent with, but do not show conclusively, that the zero-temperature critical properties are the same as those for all $p > p_{SG}(0)$ as asserted in Ref. 12. The fact that the exponent γ decreases towards its value for percolation when p approaches $p_{SG}(0)$ might indicate crossover due to the vicinity of the percolation point. However, the amplitude ratio R moves away from its percolation value. These deviations are worse for shorter series and lower dimensions. We

believe that these deviations are spurious artifacts, due to the shortness of the series which becomes more severe as T_{SG} decreases towards zero.

(5) In the lower dimensions, convergence is substantially better for intermediate dilutions than for the pure case, presumably due to a decrease in frustration. This suggests that it might be of interest to carry out simulations on a dilute system to see if this will improve convergence there too.

Finally, we have recently become aware of Ref. 32, where results for the pure three-dimensional SG are given. These are in good agreement with our critical temperature estimate and were unfortunately omitted from the comparisons in Ref. 12.

ACKNOWLEDGMENTS

APPENDIX A: THE FORM OF $g(S_i, h)$

In this appendix we discuss the form of $g(S, h)$. This derivation is valid for any symmetric distribution probability, namely, $P(J) = P(-J)$ (this appendix is a continuation of Appendix B of Ref. 20, and so we advise our readers to read this appendix for a more detailed background):

$$g(S, h) = c(h)\tilde{g}(S, h) , \tag{A1}$$

where $c(h)$ is independent of S and $\tilde{g}(S, h)$ is normalized so that it is unity for $S^\alpha = 0$,

$$c(h) = 1 + \gamma(h)n + O(n^2) , \tag{A2}$$

where

$$\gamma(h) = \lim_{n \to 0} \frac{1}{2n} \mathrm{Tr}_j \exp\left[\beta h \sum_{\alpha < \beta} S_j^\alpha S_j^\beta\right] \tilde{g}(S_j, h)^\sigma [1 - \tilde{g}(S_j, h)] . \tag{A3}$$

We only need $\tilde{g}(S_i, h)$ to leading order in n. It is determined by setting

$$\tilde{g}(S_i, h) = 1 + hav_1(S_i) + h^2[v_2(S_i)b_2 + v_1(S_i)b_1] + h^3[v_3(S_i)c_3 + v_2(S_i)c_2 + v_1(S_i)c_1]$$

$$+ h^4[v_4(S_i)d_4 + v_3(S_i)d_3 + v_2(S_i)d_2 + v_1(S_i)d_1] + \cdots , \tag{A4}$$

where for $1 \leq 2k \leq n$ we define

$$v_k(S) = \sum_{1 \leq \alpha_1 < \alpha_2 < \cdots < \alpha_{2k} \leq n} S^{\alpha_1} S^{\alpha_2} \cdots S^{\alpha_{2k}} . \tag{A5}$$

For the calculations of order h^4, we only need to evaluate the following coefficients in Eq. (A4): a, b_1, b_2, and c_1. In addition, we need to evaluate $\gamma(h)$ up to order h^4. We

obtain

$$a = xD , \tag{A6a}$$

$$b_1 = -2x(1 - \sigma x^2)D^3 , \tag{A6b}$$

$$b_2 = 3x^2 D^2 \Delta , \tag{A6c}$$

$$c_1 = \left[\frac{17x}{3}(1-3\sigma x^2+2\sigma x^3)\right]D^4$$

$$+8\sigma x^2(1-x)(1-\sigma x^2)D^5$$

$$+9\sigma x^3(1-x)D^4\Delta , \tag{A6d}$$

where $D=(1-\sigma x)^{-1}$, $\sigma=2d-1$,

$$\Delta=\frac{(1-\sigma x^2)y}{(1-\sigma y)x^2} , \tag{A6e}$$

$$x=[\tanh^2 J/k_B T]_{\text{av}} , \tag{A6f}$$

and

$$y=[\tanh^4 J/k_B T]_{\text{av}} . \tag{A6g}$$

For the distribution that we use, $x=wp$ and $y=w^2 p$.
We write $\gamma(h)=\sum_n \gamma_n h^n$ and have

$$\gamma_0=\gamma_1=0 , \tag{A7a}$$

$$\gamma_2=\tfrac{1}{4}xD^2 , \tag{A7b}$$

$$\gamma_3=-x(1-\sigma x^2)D^4 , \tag{A7c}$$

$$\gamma_4=\tfrac{1}{2}[\sigma ac_1+\tfrac{1}{2}\sigma b_1^2+\tfrac{1}{4}\sigma b_2^2+\tfrac{9}{4}\sigma(\sigma-1)a^2 b_2$$

$$-3\sigma(\sigma-1)a^2 b_1+\tfrac{17}{6}\sigma(\sigma-1)(\sigma-2)a^4+\tfrac{1}{2}c_1$$

$$+3\sigma ab_2-4\sigma ab_1+\tfrac{17}{2}\sigma(\sigma-1)a^3+\tfrac{3}{4}b_2$$

$$+\tfrac{9}{2}\sigma a^2-b_1+4\sigma a^2+\tfrac{17}{6}a] . \tag{A7d}$$

APPENDIX B:
THE DIFFERENT SUSCEPTIBILITIES
IN TERMS OF NO-FREE-END DIAGRAMS

In this appendix we discuss the form of the different susceptibilities in terms of contributions of no-free-end diagrams. This appendix is a continuation of Appendix C of Ref. 20, and so we advise our readers to read this appendix for a more detailed background. Although our series were calculated for a specific distribution function of the bonds, the NFE formulation is adequate for any other even distribution (e.g., Gaussian).

We use the notation n_b =number of bonds in the diagram Γ, n_s =number of sites in the diagram Γ, z_i =number of neighbors of site i in the diagram Γ, and $\sigma_i=z_i-1$, as well as that of Appendix A. In specifying the Γ_k^{CT} and $\delta\Gamma_k(\Gamma)$ that appear on the right-hand side of Eq. (2.1), for $k=2$, 3, and 4, it is convenient for presentation to break up their contributions. For $k=2$,

$$\Gamma_2^{\text{CT}}=D(1+x) \tag{B1a}$$

and

$$\delta\Gamma_2(\Gamma)=D^2\left[\sum_{i=1}^{n_s} z_i^2 x^2-2n_b x(1+x)\right.$$

$$+\sum_{k,l\in\Gamma}(1-\sigma_k x)(1-\sigma_l x)$$

$$\left.\times[\langle S_k S_l\rangle^2]_{\text{av}}\right] , \tag{B1b}$$

where x is defined in Eq. (A6f). We have used the distribution function

$$P(J_{ij})=(1-p)\delta_{J_{ij},0}+\frac{p}{2}(\delta_{J_{ij},J}+\delta_{J_{ij},-J}) . \tag{B2}$$

Therefore the configurational average is actually obtained as a sum over all the possible subdiagrams each weighted by its probability, namely,

$$\delta\Gamma_2(\Gamma)=D^2\left[\sum_{i=1}^{n_s} z_i^2 w^2 p^2-2n_b wp(1+wp)+\sum_{\Gamma'\in\Gamma} P(\Gamma',p)\sum_{k,l\in\Gamma'}(1-\sigma_k wp)(1-\sigma_l wp)[\langle S_k S_l\rangle^2]_{\text{av}}\right] , \tag{B3a}$$

where

$$P(\Gamma',p)=p^{n_b(\Gamma')}(1-p)^{n_b(\Gamma)-n_b(\Gamma')} . \tag{B3b}$$

Where $p=1$, then

$$P(\Gamma',1)=\begin{cases} 1 & \text{if } \Gamma'=\Gamma, \\ 0 & \text{otherwise .} \end{cases}$$

Here $n_b(\Gamma)$ and $n_b(\Gamma')$ are the number of bonds in Γ and Γ', respectively. Here and below, σ, z, n_s, and n_b are evaluated in Γ and all the correlations are evaluated in Γ'. We use the notation that

$$[\langle A_1\rangle\langle A_2\rangle\cdots\langle A_p\rangle]_{\text{av}} \tag{B4}$$

is calculated for the Hamiltonian restricted to the bonds of the cluster Γ', which we write as

$$H(\Gamma')=\sum_{\langle i,j\rangle\in\Gamma'} J_{ij}\mathbf{S}_i\cdot\mathbf{S}_j . \tag{B5}$$

Then

$$\langle A\rangle\equiv\frac{\text{Tr}e^{-\beta H(\Gamma')}A}{\text{Tr}e^{-\beta H(\Gamma')}} . \tag{B6}$$

Thus, in Eq. (B3a) (and similarly below) $[\langle S_k S_l\rangle^2]_{\text{av}}$ explicitly depends on Γ'.

Hereafter we present our results for the general even distribution. In order to obtain the explicit form for the distribution that we have used in our calculations, one should follow the example of Eqs. (B3a) and (B3b). For $k = 3$,

$$\Gamma_3^{CT} = -4D^3(1 + 3x - 3\sigma x^2 - \sigma x^3) , \tag{B7a}$$

$$\delta\Gamma_3(\Gamma) = D^3\Lambda_3(\Gamma) - 12(1-x)\delta\Gamma_2(\Gamma) , \tag{B7b}$$

where

$$\Lambda_3(\Gamma) = \left[48n_b - 12\sum_{i=1}^{n_s} z_i^2\right]x^2 + \left[4\sum_{i=1}^{n_s} z_i^3 - 12\sum_{i=1}^{n_s} z_i^2 + 16n_b\right]x^3$$

$$+ \sum_{k<l\in\Gamma}\{24(\sigma_k + \sigma_l - 1)x + 12[\sigma_k + \sigma_l - (\sigma_k + \sigma_l)^2 - 2\sigma_k\sigma_l]x^2 + 12\sigma_k\sigma_l(\sigma_k + \sigma_l)x^3\}[\langle S_k S_l\rangle^2]_{av}$$

$$-24\sum_{i<j<k\in\Gamma}(1-\sigma_i x)(1-\sigma_j x)(1-\sigma_k x)[\langle S_i S_j\rangle\langle S_i S_k\rangle\langle S_k S_i\rangle]_{av} . \tag{B8}$$

We see that for $k = 2, 3$ the generalization of the NFE formulation for the dilute case is almost trivial. We now merely use x instead of w, and the evaluation of the configurational average of the various correlation functions is more complicated. Unfortunately, for $k = 4$ we should also use averages of $\tanh^4 \beta J$ and this fact highly complicates the NFE formulation.
For $k = 4$,

$$\Gamma_4^{CT} = 34 + 68Dzx + D^3zx\{48 + [48(z-1)(z^2 - 3z + 1) - 68(z-1)(z-2)]x^2\}$$

$$+ 34D^4zx[2 - 6(z-1)x^2 - (z-1)(z^2 - 5z + 2)x^3]$$

$$+ 48D^5z(z-1)x^2[2 - zx - 2(z-1)x^2 + z(z-1)x^3] + 54D^2\Delta zx^2 + 54D^4\Delta z(z-1)x^3(2 - zx) , \tag{B9a}$$

$$\delta\Gamma_4(\Gamma) = 240D^4(1-x)^2\delta\Gamma_2(\Gamma) + D^5\Lambda_4^1(\Gamma) + D^5\Delta\Lambda_4^2(\Gamma)$$

$$+ D^4\Lambda_4^3 + D^4\Delta\Lambda_4^4 + D^4\Delta^2\Lambda_4^5 + D^3\Lambda_4^6 + D^3\Delta\Lambda_4^7 + D^3\Delta^2\Lambda_4^8 + D^2(1-\Delta)^2\Lambda_4^9 , \tag{B9b}$$

where Δ is defined in Eq. (A6e). In the absence of dilution $y = x^2$ so that $\Delta = 1$ and Eq. (B9b) reduces to Eq. (C8b) of Ref. 20. We have

$$\Lambda_4^1 = 112n_b x + \left[232\sum_{i=1}^{n_s} z_i^2 - 992n_b\right]x^2 - \left[96\sum_{i=1}^{n_s} z_i^3 + 24\sum_{i=1}^{n_s} z_i^2 - 656n_b\right]x^3$$

$$+ \left[96\sum_{i=1}^{n_s} z_i^3 - 208\sum_{i=1}^{n_s} z_i^2 + 224n_b\right]x^4$$

$$+ (1-x)\left\{\sum_{i<j\in\Gamma}\{-112 - 16[-26 + 29(\sigma_i + \sigma_j)]x + 16[18(\sigma_i + \sigma_j)^2 + 29\sigma_i\sigma_j - 8(\sigma_i + \sigma_j)]x^2\right.$$

$$-16[18\sigma_i\sigma_j(\sigma_i + \sigma_j) + 10\sigma_i\sigma_j]x^3\}[\langle S_i S_j\rangle^2]_{av}$$

$$+ 576\sum_{i<j<k\in\Gamma}[1 - (\sigma_i + \sigma_j + \sigma_k)x + (\sigma_i\sigma_j + \sigma_j\sigma_k + \sigma_k\sigma_i)x^2$$

$$\left.-\sigma_i\sigma_j\sigma_k x^3][\langle S_i S_j\rangle\langle S_j S_k\rangle\langle S_k S_i\rangle]_{av}\right\} , \tag{B10}$$

$$\Lambda_4^2 = -432n_b x^2 + 216\sum_{i=1}^{n_s} z_i^2 x^3 - \left[216\sum_{i=1}^{n_s} z_i^2 - 432n_b\right]x^4$$

$$+ (1-x)\sum_{i<j\in\Gamma}[432x - 432(\sigma_i + \sigma_j)x^2 + 432\sigma_i\sigma_j x^3][\langle S_i S_j\rangle^2]_{av} , \tag{B11}$$

$$\Lambda_4^3 = 108 \left[\sum_{i=1}^{n_s} z_i^2 - 6n_b \right] x^2 - \left[136 \sum_{i=1}^{n_s} z_i^3 - 396 \sum_{i=1}^{n_s} z_i^2 + 456n_b \right] x^3$$

$$+ \left[34 \sum_{i=1}^{n_s} z_i^4 - 28 \sum_{i=1}^{n_s} z_i^3 - 66 \sum_{i=1}^{n_s} z_i^2 + 120n_b \right] x^4$$

$$+ \sum_{i<j\in\Gamma} [(216[2-(\sigma_i+\sigma_j)]x + [-64-384(\sigma_i+\sigma_j)+408(\sigma_i+\sigma_j)^2]x^2$$

$$+ \{192\sigma_i\sigma_j[1-(\sigma_i+\sigma_j)]-136(\sigma_i+\sigma_j)^3-120(\sigma_i+\sigma_j)^2+80(\sigma_i+\sigma_j)\}x^3$$

$$+ \sigma_i\sigma_j[432+136(\sigma_i+\sigma_j)^2+216(\sigma_i+\sigma_j)-176\sigma_i\sigma_j]x^4][\langle S_iS_j\rangle^2]_{av}$$

$$+ \{108-216[1+(\sigma_i+\sigma_j)]x+108[1+3(\sigma_i+\sigma_j)+(\sigma_i+\sigma_j)^2+2\sigma_i\sigma_j]x^2$$

$$- 108[2\sigma_i\sigma_j+(\sigma_i+\sigma_j)^2+(\sigma_i+\sigma_j)(1+2\sigma_i\sigma_j)]x^3+108\sigma_i\sigma_j[1+(\sigma_i+\sigma_j)+\sigma_i\sigma_j]x^4\}[\langle S_iS_j\rangle^4]_{av}]$$

$$+ \sum_{i<j<k\in\Gamma} \{[576-384(\sigma_i+\sigma_j+\sigma_k)]x+192[(\sigma_i+\sigma_j+\sigma_k)^2(\sigma_i\sigma_j+\sigma_j\sigma_k+\sigma_k\sigma_i)-2(\sigma_i+\sigma_j+\sigma_k)]x^2$$

$$+ 192[(\sigma_i\sigma_j+\sigma_j\sigma_k+\sigma_k\sigma_i)-3\sigma_i\sigma_j\sigma_k-(\sigma_i+\sigma_j+\sigma_k)(\sigma_i\sigma_j+\sigma_j\sigma_k+\sigma_k\sigma_i)]x^3$$

$$+ 192\sigma_i\sigma_j\sigma_k(\sigma_i+\sigma_j+\sigma_k)x^4\}[\langle S_iS_j\rangle\langle S_jS_k\rangle\langle S_kS_i\rangle]_{av}$$

$$+216 \sum_{i<j;k\neq i,j\in\Gamma} \{1-(1+\sigma_i+\sigma_j+2\sigma_k)x+[(2\sigma_k+1)(\sigma_i+\sigma_j)+\sigma_k(1+\sigma_k)+\sigma_i\sigma_j]x^2$$

$$- [(\sigma_k+\sigma_k^2)(\sigma_i+\sigma_j)+\sigma_i\sigma_j(2\sigma_k+1)]x^3+\sigma_k(\sigma_k+1)\sigma_i\sigma_jx^4\}$$

$$\times [\langle S_iS_k\rangle^2\langle S_jS_k\rangle^2]_{av}$$

$$+ \sum_{i<j<k<l\in\Gamma} (1-x\sigma_i)(1-x\sigma_j)(1-x\sigma_k)(1-x\sigma_l)$$

$$\times \{288([\langle S_iS_j\rangle\langle S_jS_k\rangle\langle S_kS_l\rangle\langle S_lS_i\rangle]_{av}+[\langle S_iS_k\rangle\langle S_kS_j\rangle\langle S_jS_l\rangle\langle S_lS_i\rangle]_{av}$$

$$+ [\langle S_iS_j\rangle\langle S_jS_l\rangle\langle S_lS_k\rangle\langle S_kS_i\rangle]_{av})$$

$$- 96([\langle S_iS_jS_kS_l\rangle\langle S_iS_j\rangle\langle S_kS_l\rangle]_{av}+[\langle S_iS_jS_kS_l\rangle\langle S_iS_k\rangle\langle S_jS_l\rangle]_{av}$$

$$+ [\langle S_iS_jS_kS_l\rangle\langle S_iS_l\rangle\langle S_jS_k\rangle]_{av})$$

$$+ 72([\langle S_iS_j\rangle^2\langle S_kS_l\rangle^2]_{av}+[\langle S_iS_k\rangle^2\langle S_jS_l\rangle^2]_{av}$$

$$+ [\langle S_iS_l\rangle^2\langle S_jS_k\rangle^2]_{av})+24[\langle S_iS_jS_kS_l\rangle^2]_{av}\} , \tag{B12}$$

$$\Lambda_4^4 = 108 \left[3n_bx^2 + \left[\sum_{i=1}^{n_s} z_i^2 - 5n_b \right] x^3 - \left[\sum_{i=1}^{n_s} z_i^3 - 2\sum_{i=1}^{n_s} z_i^2 + 2n_b \right] x^4 \right]$$

$$+ 108 \left\{ \sum_{i<j\in\Gamma} (\{-4x+4x^2+2[(\sigma_i+\sigma_j)^2-(\sigma_i+\sigma_j)]x^3-2\sigma_i\sigma_j(\sigma_i+\sigma_j)x^4\}[\langle S_iS_j\rangle^2]_{av} \right.$$

$$+ \{2x-[2+3(\sigma_i+\sigma_j)]x^2+[(\sigma_i+\sigma_j)^2+2(\sigma_i+\sigma_j)+2\sigma_i\sigma_j]x^3$$

$$- [2\sigma_i\sigma_j+(\sigma_i+\sigma_j)\sigma_i\sigma_j]x^4\}[\langle S_iS_j\rangle^4]_{av})$$

$$\left. +2 \sum_{i<j;k\neq i,j\in\Gamma} [x-(\sigma_i+\sigma_j+\sigma_k)x^2+(\sigma_i\sigma_j+\sigma_j\sigma_k+\sigma_k\sigma_i)x^3-\sigma_i\sigma_j\sigma_kx^4][\langle S_iS_k\rangle^2\langle S_jS_k\rangle^2]_{av} \right\} , $$

$$\tag{B13}$$

$$\Lambda_4^5 = -108n_bx^3+54 \left[\sum_{i=1}^{n_s} z_i^2 - 2n_b \right] x^4 + 108 \sum_{i<j\in\Gamma} [x^2-(\sigma_i+\sigma_j)x^3+\sigma_i\sigma_jx^4][\langle S_iS_j\rangle^4]_{av} , \tag{B14}$$

$$\Lambda_4^6 = 108 \left[\sum_{i=1}^{n_s} z_i^2 - 2n_b \right] x^3 + 108 \left\{ \sum_{i<j\in\Gamma} (-[2(\sigma_i+\sigma_j)x^2 - 4\sigma_i\sigma_j x^3][\langle S_iS_j \rangle^2]_{\mathrm{av}} \right.$$

$$+ \{2x - 2[1+(\sigma_i+\sigma_j)]x^2 + [(\sigma_i+\sigma_j)^2 - 2\sigma_i\sigma_j + (\sigma_i+\sigma_j)]x^3\}[\langle S_iS_j \rangle^4]_{\mathrm{av}})$$

$$\left. -2 \sum_{i<j;k\neq i,j\in\Gamma} [-x+(\sigma_i+\sigma_j)x^2 - \sigma_i\sigma_j x^3][\langle S_iS_k \rangle^2 \langle S_jS_k \rangle^2]_{\mathrm{av}} \right\}, \qquad (B15)$$

$$\Lambda_4^7 = -108 \left[\sum_{i=1}^{n_s} z_i^2 - n_b \right] x^3$$

$$+ 108 \left\{ \sum_{i<j\in\Gamma} ([2(\sigma_i+\sigma_j)x^2 - 4\sigma_i\sigma_j x^3][\langle S_iS_j \rangle^2]_{\mathrm{av}} \right.$$

$$+ \{-2x + 2[2+(\sigma_i+\sigma_j)]x^2 + [-(\sigma_i+\sigma_j)^2 + 2\sigma_i\sigma_j - 2(\sigma_i+\sigma_j)]x^3\}[\langle S_iS_j \rangle^4]_{\mathrm{av}})$$

$$\left. +2 \sum_{i<j;k\neq i,j\in\Gamma} [-x+(\sigma_i+\sigma_j)x^2 - \sigma_i\sigma_j x^3][\langle S_iS_k \rangle^2 \langle S_jS_k \rangle^2]_{\mathrm{av}} \right\}, \qquad (B16)$$

$$\Lambda_4^8 = 108 n_b x^3 + 108 \sum_{i<j\in\Gamma} [-2x^2 + (\sigma_i+\sigma_j)x^3][\langle S_iS_j \rangle^4]_{\mathrm{av}}, \qquad (B17)$$

$$\Lambda_4^9 = 108 \sum_{i<j\in\Gamma} x^2 [\langle S_iS_j \rangle^4]_{\mathrm{av}}. \qquad (B18)$$

*Present address: Department of Physics, Stanford University, Stanford, CA 94305.

[1] S. F. Edwards and P. W. Anderson, J. Phys. F 5, 965 (1975).

[2] M. J. Stephen and G. S. Grest, Phys. Rev. Lett. 38, 567 (1977).

[3] M. R. Giri and M. J. Stephen, J. Phys. C 11, L541 (1978).

[4] A. Aharony, J. Phys. C 11, L457 (1978).

[5] B. Southern, A. P. Young, and P. Pfeuty, J. Phys. C 12, 683 (1979).

[6] A. Aharony and P. Pfeuty, J. Phys. C 12, L125 (1979).

[7] A. Aharony and K. Binder, J. Phys. C 13, 4091 (1980).

[8] A. Benyoussef and N. Boccara, J. Phys. C 16, 1901 (1983); Phys. Lett. 93A, 351 (1983).

[9] R. G. Palmer and F. T. Bantilan, J. Phys. C 28, 171 (1985).

[10] A. B. Harris, J. Phys. A 20, L1011 (1987).

[11] A. J. Bray and S. Feng, Phys. Rev. B 36, 8456 (1987).

[12] L. Klein, J. Adler, A. Aharony, A. B. Harris, and Y. Meir, Phys. Rev. B 40, 4824 (1989); see corrected tabulation of series in 43, 13 684 (1991).

[13] D. S. Stauffer and A. Aharony, Introduction to Percolation Theory (Taylor & Francis, London, 1992).

[14] D. E. Khmel'nitzkii, Zh. Eksp. Teor. Fiz. 68, 1960 (1975) [Sov. Phys. JETP 41, 981 (1976)]; G. Grinstein and A. H. Luther, Phys. Rev. B 13, 1329 (1976); A. Aharony, ibid. 13, 2092 (1976).

[15] A. B. Harris, J. Phys. C 7, 1671 (1974).

[16] J. Adler, Physica A 177, 45 (1991).

[17] H. Fried and M. Schick, Phys. Rev. B 38, 954 (1989).

[18] A raised p_c value and different critical exponents have been measured for quantum percolation by Y. Meir, A. Aharony, and A. B. Harris, Europhys. Lett. 10, 275 (1989). Different exponents were found for the dilute quantum Heisenberg model by C. C. Wan, A. B. Harris, and J. Adler, J. Appl. Phys. 69, 5191 (1991); C. C. Wan and A. B. Harris (unpublished).

[19] R. N. Bhatt and A. P. Young, Phys. Rev. Lett. 54, 924 (1985);

A. T. Ogielski, Phys. Rev. B 32, 7384 (1985); R. R. P. Singh and S. Chakravarty, ibid. 36, 559 (1987).

[20] L. Klein, J. Adler, A. Aharony, A. B. Harris, and Y. Meir, Phys. Rev. B 43, 11 249 (1991).

[21] A. Aharony, Phys. Rev. B 22, 400 (1980).

[22] V. Privman, P. C. Hohenberg, and A. Aharony, in Phase Transitions and Critical Phenomena, edited by C. Domb and J. Lebowitz (Academic, New York, 1991), Vol. 14.

[23] See AIP document No. PAPS PRBMD-49-8830-15 for 15 pages of Tables I–IV. Order by PAPS number and journal reference from the American Institute of Physics, Auxiliary Publication Service, 500 Sunnyside Boulevard, Woodbury, New York 11797-2999. The price is $1.50 for each microfiche (60 pages) or $5.00 for photocopies of up to 30 pages, and $0.15 for each additional page over 30 pages. Airmail additional. Make checks payable to the American Institute of Physics.

[24] A. B. Harris, Phys. Rev. B 26, 337 (1982); A. B. Harris and Y. Meir, ibid. 36, 1840 (1987).

[25] D. S. Gaunt and A. J. Guttmann, in Phase Transitions and Critical Phenomena, edited by C. Domb and J. Lebowitz (Academic, New York, 1991), Vol. 15.

[26] J. Adler, I. Chang, and S. Shapira, Int. J. Mod. Phys. C 4, 1007 (1993).

[27] J. Adler, M. Moshe, and V. Privman, Phys. Rev. B 26, 1411 (1982); J. Adler, M. Moshe, and V. Privman, J. Phys. A 14, L363 (1981).

[28] J. Adler, M. Moshe, and V. Privman, in Annals of the Israel Physical Society, edited by G. Deutscher, R. Zallen, and J. Adler (Hilger, London, 1983), Vol. 3.

[29] J. Adler and V. Privman, J. Phys. A 14, L463 (1981).

[30] J. Adler, Y. Meir, A. Aharony, and A. B. Harris, Phys. Rev. B 41, 9183 (1990).

[31] H. Maletta and P. Convert, Phys. Rev. Lett. 42, 108 (1979).

[32] J. S. Wang and R. H. Swendsen, Phys. Rev. B 37, 7745 (1988).